Temperature-dependent thermal conductivity in silicon nanostructured materials studied by the Boltzmann transport equation

Giuseppe Romano, Keivan Esfarjani, David A. Strubbe, David Broido, and Alexie M. Kolpak

Temperature-dependent thermal conductivity in silicon nanostructured materials studied by the Boltzmann Transport Equation

Giuseppe Romano

Department of Mechanical Engineering, Massachusetts Institute of Technology,
77 Massachusetts Avenue, Cambridge, MA 02139 and
Department of Physics, Boston College, Chestnut Hill, MA 02467, USA[*]

Keivan Esfarjani

Department of Mechanical and Aerospace Engineering,
Rutgers University, Piscataway, NJ 08854, USA

David A. Strubbe

Department of Materials Science, Massachusetts Institute of Technology,
77 Massachusetts Avenue, Cambridge, MA 02139

David Broido

Department of Physics, Boston College, Chestnut Hill, MA 02467, USA[*]

Alexie M. Kolpak

Department of Mechanical Engineering, Massachusetts Institute of Technology,
77 Massachusetts Avenue, Cambridge, MA 02139

  Nanostructured materials exhibit low thermal conductivity because of the additional scattering due to phonon-boundary interactions. As these interactions are highly sensitive to the mean free path (MFP) of phonons, MFP distributions in nanostructures can be dramatically distorted relative to bulk. Here we calculate the MFP distribution in periodic nanoporous Si for different temperatures, using the recently developed MFP-dependent Boltzmann Transport Equation. After analyzing the relative contribution of each phonon branch to thermal transport in nanoporous Si, we find that at room temperature optical phonons contribute 17% to heat transport, compared to 5% in bulk Si. Interestingly, we observe a constant thermal conductivity over the range 200 K $< T <$ 300 K. We attribute this behavior to the ballistic transport of acoustic phonons with long intrinsic MFP and the temperature dependence of the heat capacity. Our findings, which are in qualitative agreement with the temperature trend of thermal conductivities measured in nanoporous Si-based systems, shed light on the origin of the reduction of thermal conductivity in nanostructured materials, and demonstrate the necessity of multiscale heat transport engineering, in which the bulk material and geometry are optimized concurrently.

I. INTRODUCTION

The quest for high-efficiency thermoelectric materials may be advanced by using the ability of nanostructures to suppress heat transport by several orders of magnitude with respect to bulk without degrading electrical transport significantly.[1] This phenomenon is based on the fact that phonon mean free paths (MFPs) are generally larger than electron MFPs; consequently, heat transport exhibits stronger size effects. The extent of the suppression of phonon transport depends on the ratio between the intrinsic phonon MFP and the characteristic length of the nanostructure, L_c. This ratio is known as the Knudsen number (Kn). When L_c is much smaller than MFP, *i.e.* for small Kn, phonon interactions with boundaries are negligible. In this regime, heat transport reduction is only due to geometrical effects, such as material removal in nanoporous materials, while phonon-boundary scattering is minimal. Therefore, heat transport is dominated by intrinsic scattering. On the other hand, for high Kn, scattering is dominated by phonon-boundary interactions. Within this regime, the phonon MFPs in the nanostructure approach L_c and the phonons are considered to travel ballistically. The intermediate regime (*i.e.* $Kn \approx 1$) is often referred to as the quasi-ballistic regime.

This analysis implicitly assumes single-MFP materials, but in most materials, there is a wide distribution of phonon MFPs, which in some cases span several orders of magnitude. For example, first-principles calculations for Si show that about half of the heat is carried by phonons with MFPs larger than 1 μm.[2] Recent experimental measurements showing a reduction in thermal conductivity of Si membranes with microscale pores[3] provide support for these computational results. Together, they suggest that an accurate analysis of thermal transport in nanostructures should include the actual bulk MFP distribution.

In bulk Si, the optical and acoustic phonons have very different MFP distributions.[2] Optical phonons have relatively low MFPs because their dispersion curves are flatter than those of acoustic phonons, which by contrast have large MFPs. This effect has important consequences on thermal conductivity. First-principles calculations show that optical phonons contribute only 5% to the total thermal conductivity of Si, while the remaining 95% is dominated by acoustic phonons.[2] As a result, optical phonons are often neglected when calculating nanoscale heat transport in Si. However, in nanostructures, heat carried by optical phonons is only slightly reduced while acoustic phonons can be strongly suppressed, making the two contributions comparable.

We recall that the phonon MFP is given by $\Lambda = |\mathbf{v}|\tau$, where $\mathbf{v}$ is the phonon group velocity for a given polarization and frequency and τ is the scattering time. In bulk materials, the scattering events comprise several mechanisms, including three-phonon scattering, phonon-isotope scattering, electron-phonon scattering and interaction with defects.[4] The scattering rates related to these events, which we define here as intrinsic events, are typically assumed independent and summed up following the Matthiessen's rule. In presence of boundaries, phonon MFPs are modified for two reasons. First, phonon-boundary interactions modify the total scattering time. Secondly, coherent effects may affect phonon group velocities via the change in the dispersion curves. As we will see later in the text, our study focuses on nanoporous-Si (np-Si) with periodicity of about 10 nm. The importance of coherence effects in such systems has been assessed in another recent study, where Monte Carlo simulations were used to compute thermal transport in np-Si membranes.[5] Their conclusion was, however, that incoherent effects can fully explain the remarkably low thermal conductivity in these systems.[6] On the other side, a recent work attempts to quantify the effect of coherence effects in periodic structures at room temperature.[7] In this study, the coherence regime is accounted for band-folding effects and a hybrid coherent/incoherent model was able to partially explain the remarkably low thermal conductivities obtained in their samples. It is clear, therefore, that the influence of phonon phase-conserving phenomena in such structures is still under debate. In this work, however, we focus on assessing the temperature dependence of heat transport in nanostructures when heat reduction is dominated by incoherent effects. For this reason, we will compare our results qualitatively with experiments on disordered pores, where coherence effects unlikely take place.

A simple model for phonon-boundary scattering was devised by Casimir in 1938.[8] Within the Casimir approach, the scattering rates related to phonon-boundary scattering are considered independent from the intrinsic mechanisms and the MFP induced by such events is the same as the material's characteristic length. Using the Casimir model, Tian *et al.*[9] concluded that optical phonons in Si nanowires contribute over 20% to the total thermal conductivity at room temperature. When dealing with complex boundaries, the Casimir approach fails for two reasons.[10] First, it assumes that the characteristic length is known a *priori*, while in most materials with complex geometry this quantity is unknown. Secondly, a portion of the MFP distribution may lie in the diffusive or quasi-ballistic regime.

In this work, we use the MFP-dependent Boltzmann Transport Equation (MFP-BTE)[11] to calculate heat transport in nanoporous materials and provide the relative contribution of each phonon branch to the thermal conductivity as a function of temperature. The use of the BTE enables treatment of complex geometries with a good level of predictive power. We focus on np-Si with aligned pores with square cross section and a periodicity of 10 nm, and consider the temperature range $100\,\mathrm{K} - 300\,\mathrm{K}$. We show that at room temperature the thermal conductivity in np-Si is suppressed by more than one order of magnitude with respect to bulk Si, with longitudinal optical (LO) phonons contributing more than 15% to the total heat transport. This result is in agreement with the previous qualitative discussion above.

Further, we find that the thermal conductivity of np-Si exhibits a plateau over the temperature range $200\,\mathrm{K} - 300\,\mathrm{K}$. We demonstrate that this arises from two effects: first, as most of the acoustic phonons travel ballistically because of their large Kn, their MFPs in np-Si are constrained by the characteristic length of the material, and therefore are not reduced by increasing temperature. Second, in this temperature range, the heat carried by optical phonons changes weakly with temperature in bulk Si itself, inducing similar behavior to np-Si. By revealing the microscopic mechanisms leading to the reduction in heat conduction, our findings may enable new approaches for engineering high-efficiency thermoelectric devices.

II. METHOD

To compute the reduction of heat transport in nanostructures, we employ the concept of the "suppression function," $S(\Lambda)$, which, in the context of the steady-state BTE, defines the departure from diffusive transport in terms of the MFP distribution function:[11]

$$S(\Lambda) = \frac{K_p^{\mathrm{nano}}(\Lambda)}{K_p^{\mathrm{bulk}}(\Lambda)}, \tag{1}$$

where $K_p^{\mathrm{bulk}}(\Lambda)$ and $K_p^{\mathrm{nano}}(\Lambda)$ are the bulk MFP distributions for branch p in bulk Si and np-Si, respectively. Within the relaxation time approximation, the effective thermal conductivity for each phonon branch can be written as

$$\kappa_p^{\mathrm{nano}} = \int_0^\infty K_p^{\mathrm{nano}}(\Lambda)d\Lambda = \int_0^\infty K_p^{\mathrm{bulk}}(\Lambda)S(\Lambda)d\Lambda. \tag{2}$$

The total thermal conductivity is then given by $\kappa^{\mathrm{nano}} = \sum_p \kappa_p^{\mathrm{nano}}$. In the case of purely diffusive transport, the suppression function is MFP-independent and Eq. 2 leads to the diffusive thermal conductivity $\kappa^{\mathrm{nano}} = \kappa^{\mathrm{bulk}}g$, where g is a function that depends only on the material geometry and κ^{bulk} is the bulk thermal conductivity. The bulk MFP distribution at different temperatures can be obtained either experimentally through MFP reconstruction techniques[12] or computationally. In this work we adopt a first-principles approach based on Density Functional Theory (DFT) and the linearized BTE.[2,13] The bulk MFP distribution is computed via $K_p^{\mathrm{bulk}}(\Lambda) = \frac{\partial \alpha_p^{\mathrm{bulk}}(\Lambda)}{\partial \Lambda}$, where $\alpha_p^{\mathrm{bulk}}(\Lambda)$ is the cumulative thermal conductivity. We recall that the cumulative thermal conductivity is the thermal conductivity of phonons whose MFPs are below a given Λ.[14,15] We note that $\alpha_p^{\mathrm{bulk}}(\Lambda)$ does not include boundary scattering. For this reason, in rest of this study, we will refer to such a result as bulk-BTE. Details on the calculation of $\alpha_p^{\mathrm{bulk}}(\Lambda)$ can be found in the Appendix.

The suppression function can be obtained in different ways, depending on the system and the required accuracy. In some cases, such in nanowires and thin films, $S(\Lambda)$ can be obtained analytically within a reasonable level of accuracy.[16] However, most of the analytical derivations are based on the "gray" approximation, which assumes phonon dispersions described by a single group velocity. Furthermore, formulae for the suppression function are limited to simple geometries. In this work we therefore employ a recently developed formulation of the BTE that requires only the bulk MFP distribution $K_p^{\mathrm{bulk}}(\Lambda)$.[11] This method, MFP-BTE, has the same accuracy as the the commonly used frequency-dependent approach (FD-BTE), provided that we consider small applied temperature gradients, $\Delta T/L$, where ΔT is the applied difference of temperature and L is the distance between the hot and cold contact. The key equation of the MFP-BTE is the integro-differential equation

$$\Lambda \mathbf{s} \cdot \nabla \tilde{T}(\Lambda) + \tilde{T}(\Lambda) = \gamma \sum_p \int_0^\infty \frac{K_p^{\mathrm{bulk}}(\Lambda')}{\Lambda'^2} < \tilde{T}(\Lambda') > d\Lambda', \tag{3}$$

where $\tilde{T}(\mathbf{r}, \mathbf{s}, \Lambda)$ represents the local temperature of phonons travelling along the direction $\mathbf{s}$, depending only on the MFP Λ.[11] In Eq. 3, $\mathbf{s}$ is the phonon propagation direction and γ a material property given by $\gamma = \left[\sum_p \int_0^\infty \frac{K_p^{\mathrm{bulk}}(\Lambda)}{\Lambda^2} d\Lambda\right]^{-1} = 2.2739 \times 10^{-17}\ \mathrm{KW^{-1}m^3}$ for Si.[11] The notation $< x >$ stands for an angular average. The right-hand-side of Eq. 3 is the effective lattice temperature $T_L(\mathbf{r})$,[11] which does not depend on Λ explicitly, and provides an average of the local energy of phonons. We note that both $\tilde{T}$ and T_L are normalized to ΔT. Once Eq. 3 is solved, the suppression function can be computed via the following integral over either the cold or hot contact:

$$S(\Lambda) = \frac{3L}{\Lambda A} \int_\Gamma < \tilde{T}\mathbf{s} \cdot \mathbf{n}_s > dS, \tag{4}$$

where Γ is the surface of the contact having normal $\mathbf{n}_s$ and area A. The MFP-BTE is solved for a set of 30 MFPs, uniformly spaced on a logarithmic scale from about 0.1 nm to 100 μm. The spatial discretization is achieved by means of the finite-volume approach whereas the solid angle is discretized by means of the discrete-ordinate method.[17]

Our simulation domain consists of a square unit cell, containing one square pore, to which a difference of temperature $\Delta T = 1$ K is applied. Periodic boundary conditions are applied to both the longitudinal and transverse direction of heat flux, $\mathbf{n_f}$, which is enforced by applying a difference of temperature ΔT along $\mathbf{n_f}$, *i.e.*

$$\tilde{T}(\Lambda, \mathbf{s}, \mathbf{r}) - \tilde{T}(\Lambda, \mathbf{s}, \mathbf{r} + \mathbf{P}) = (\mathbf{n} \cdot \mathbf{n_f})\Delta T, \tag{5}$$

where $\mathbf{r}$ runs along the faces of the unit cell, $\mathbf{n}$ is the normal to the boundary pointing outside the domain and $\mathbf{P}$ is the periodicity vector. It is straightforward to show that along the direction perpendicular to the heat flux, no difference of temperature is imposed. We assume that we have an infinite material along the directions orthogonal to the pore plane. To properly set the boundary conditions along the pores' surface, we note that the zero-flux conditions can be achieved by imposing that the total phonon flux incoming to the surface (P^-) be equal to the outgoing flux (P^+). Within the MFP-BTE formalism, the phonon flux along a direction $\mathbf{s}$ is given by $\mathbf{J}(\Lambda, \mathbf{s}, \mathbf{r}) = \mathbf{s}\tilde{T}(\Lambda, \mathbf{s}, \mathbf{r})K_p^{\text{bulk}}/\Lambda$.[11] The condition $P^+ = P^-$ is then obtained by

$$\sum_p \int_0^\infty \int_{\mathbf{s} \cdot \mathbf{n} < 0} \frac{K_p^{\text{bulk}}(\Lambda)}{\Lambda} \tilde{T}^- \mathbf{s} \cdot \mathbf{n} d\Omega d\Lambda = \sum_p \int_0^\infty \int_{\mathbf{s} \cdot \mathbf{n} \geq 0} \frac{K_p^{\text{bulk}}(\Lambda)}{\Lambda} \tilde{T}^+ \mathbf{s} \cdot \mathbf{n} d\Omega d\Lambda \tag{6}$$

where $\mathbf{s} \cdot \mathbf{n} < 0$ and $\mathbf{s} \cdot \mathbf{n} \geq 0$ stand for phonons incident to the surface and phonons leaving the surface, respectively. Here we assume that the surface scatters phonons diffusively so that phonons leaving the surface do not bear memory of their direction and MFP before scattering with the surface. Practically, the scattered phonons are uniformly distributed in angular space. In Eq. 6, the term $d\Omega$ is the infinitesimal solid angle. This condition is met by setting $\tilde{T}^-$ to the following average:[18]

$$\tilde{T}^- = P^+ \left[\sum_p \int_0^\infty \int_{\mathbf{s} \cdot \mathbf{n} < 0} \frac{K_p^{\text{bulk}}(\Lambda)}{\Lambda} \mathbf{s} \cdot \mathbf{n} d\Omega d\Lambda \right]^{-1} \tag{7}$$

We note that this assumption must be used with caution, especially at very low temperatures, as some phonons can be reflected specularly depending on the roughness of the boundary. However, in this work we assume surfaces have sufficient roughness that specularity effects can be neglected in the range of temperature considered. Details on the surface specularity effects on thermal transport can be found in Ref. 19.

III. RESULTS AND DISCUSSION

We have first applied the MFP-BTE to bulk Si, obtaining exactly the same results as those from bulk-BTE, as there are no boundaries scattering phonons. The simulation domain for the np-Si cases has periodicity $L = 10$ nm and porosities $\phi = 0.05$ and $\phi = 0.25$. We recall that the porosity is the amount of material removal, which, for square pores, is simply $\phi = L_p^2/L^2$, with L_p being the size of the pore. The heat flow is enforced along the in-plane direction. In Fig. 1-a, the magnitude of the thermal flux for $\phi = 0.25$ is shown. As expected, heat travels mostly in the regions between pores along the direction of the imposed gradient of temperature. The value for the thermal conductivities at room temperature for bulk Si is about 143 Wm^{-1}K^{-1}, whereas for the np-Si cases it is only 15.0 Wm^{-1}K^{-1} and 5.65 Wm^{-1}K^{-1} for porosities $\phi = 0.05$ and $\phi = 0.25$, respectively. This reduction of one order of magnitude with respect to bulk is in quantitative agreement with previous studies,[11,20] and demonstrates the high ability of nanostructures to tune thermal transport.

We now analyze the relative contribution of each phonon branch to the total thermal conductivity. Fig. 2-a shows the normalized cumulative thermal conductivity for bulk Si at $T = 300$ K. As expected, acoustic phonons contribute most to the thermal conductivity, while optical phonon contributions are small. In particular, the two transverse acoustic (TA) branches and longitudinal acoustic (LA) branch contribute approximately one third each to the total thermal conductivity. The figure also shows that the LO phonons contribute 5% to thermal transport, while the transverse optical (TO) phonons have a negligible contribution. However, the LO phonons start to contribute significantly in np-Si, reaching 16% and 17% of the total thermal conductivity for the cases with $\phi = 0.05$ (Fig. 2-b) and $\phi = 0.25$ (Fig. 2-c), respectively. The TO contribution remains negligible.

The roughly four-fold increase in the relative contribution of LO phonons can be better understood by analyzing the MFP distributions in relation to L_c. According to Ref. 20, in porous materials L_c can be defined as the pore-pore distance in the direction orthogonal to thermal flux. The pore-pore distance in an array of square aligned pores is
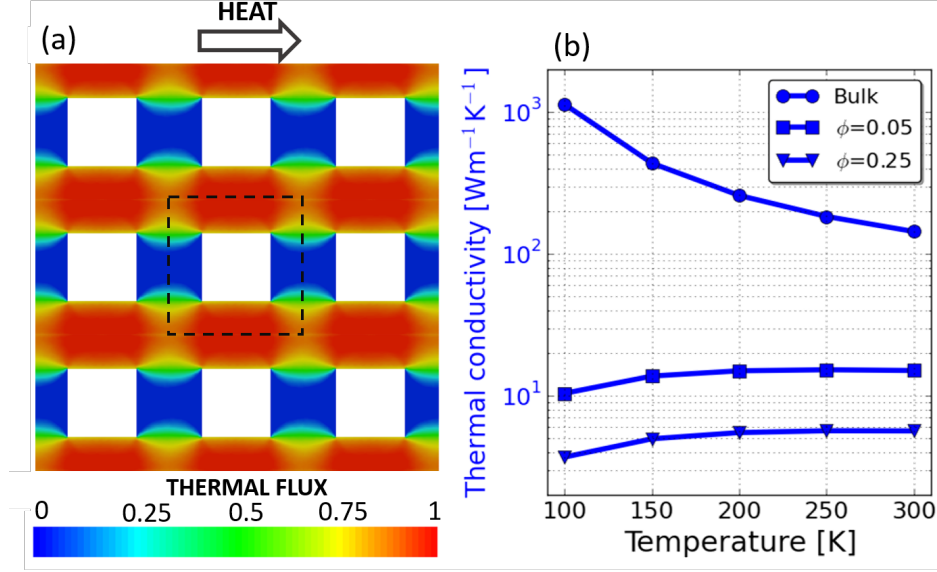
FIG. 1. a) Periodically aligned square pores (with porosity $\phi = 0.25$ and $L_c = 10$ nm), subjected to a difference of temperature. The magnitude of thermal flux, which is normalized to its maximum value, shows that phonons travel mostly in areas between pores along the direction of the temperature gradient. b) Thermal conductivity versus temperature for bulk Si and np-Si with porosities $\phi = 0.25$ and $\phi = 0.05$.

related to the porosity via $L_c = L(1 - \sqrt{\phi})$, which leads to the values 5 nm and 7.76 nm for $\phi = 0.25$ and $\phi = 0.05$, respectively. The characteristic length dictates the transport regime of phonons with a given MFP. Figure 2-a shows that the maximum MFP of LO phonons contributing to the thermal conductivity is around 20 nm, while acoustic phonons have MFPs up to 10 μm. As a result, optical phonons, which generally have MFPs similar to L_c, are less suppressed than acoustic phonons. For $\phi = 0.25$, the characteristic length is even smaller and, consequently, the relative LO phonon contribution increases (up to 17%, as shown in Fig. 2-c).

When L_c is larger (e.g. 100 nm), the effect of the nanostructure on optical phonons becomes negligible, but most acoustic phonons are still suppressed. In this case, it is possible to have a "reversal effect," in which optical phonons are the main contribution to the thermal conductivity. For macroscopic samples, e.g. $L_c > 100$ μm, the thermal conductivity approaches the diffusive value predicted by the Fourier model and the MFP distributions are restored to the bulk ones times the geometric factor, g, that depends only on the geometry. For aligned porous materials, the geometry factor can be well approximated by $g = \frac{1-\phi}{1+\phi}$.[21] This approximation was validated against finite-element modeling of diffusive heat conduction.[19]

This finding has important consequences for optimizing nanostructured thermoelectric materials. Typically, the bulk thermoelectric materials and the geometry of the nanostructure are optimized separately.[1] Here we suggest that both macro and nanoscale have to be considered concurrently. The following example helps clarify this point. Let us assume that we have two "gray" materials, A and B, with average MFPs Λ_A and Λ_B, respectively. We further assume that the thermal conductivity of material B is larger than that of material A. We consider a nanostructure with $\Lambda_A \ll L_c \ll \Lambda_B$. Material B will undergo strong phonon suppression whereas heat transport in material A will still be in the diffusive regime. It is clear therefore that, with a sufficiently large Λ_B, material B exhibits lower thermal conductivity than that of material A, making it more appealing for thermoelectrics. Similar conclusions can be drawn for non-gray materials.

We now investigate the temperature dependence of thermal conductivity in the range 200 K < T < 300 K. All the results shown below refer to the case with $\phi = 0.25$. Similar conclusions can be drawn for the case with $\phi = 0.05$. As shown in Fig. 1, the thermal conductivity of np-Si exhibits little change in this temperature range, whereas it decreases as $1/T$ due to Umklapp scattering in bulk Si.[2,13] This behavior arises from the very large Kn of acoustic phonons, which therefore travel ballistically. According to Fig. 3, when the temperature approaches 200 K, the bulk MFP of high-Kn acoustic phonons becomes even longer, further enhancing the ballistic effect. In np-Si, the MFP of these phonons are constrained to be equal to L_c. In this regime, heat transport is governed by heat capacity, which, according to Fig. 4-a does not change significantly. On the other side, the MFP distribution in the region around L_c, which is shaded in Fig. 3, remains essentially unaltered over this temperature range. As a result, the thermal
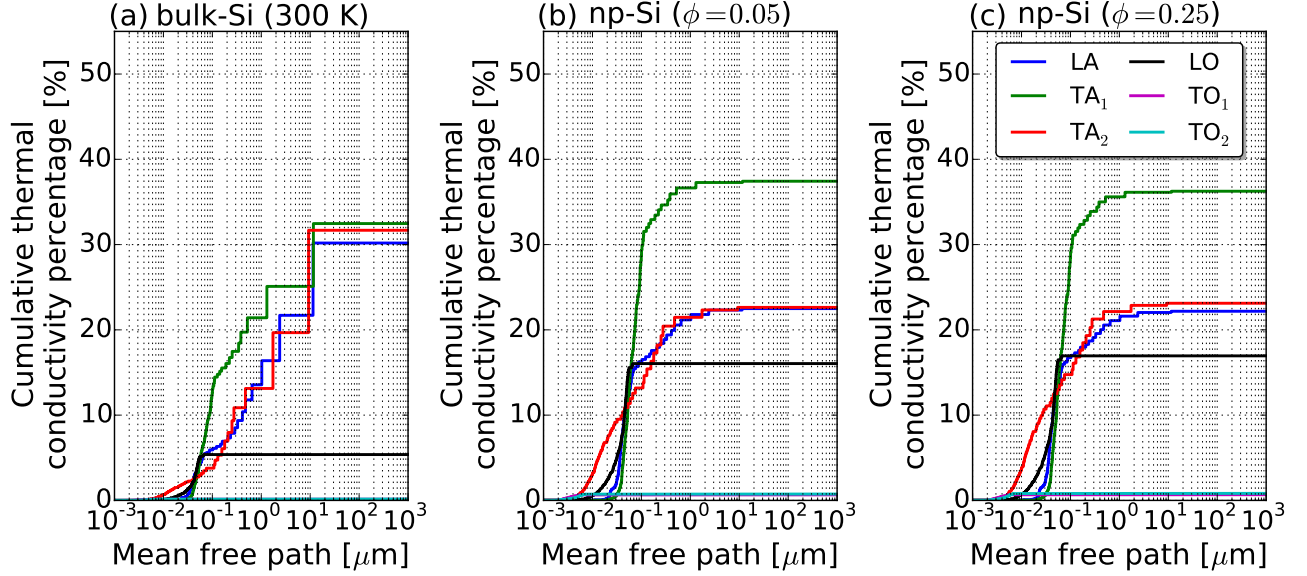
FIG. 2. Cumulative thermal conductivity at $T = 300$ K for a) bulk Si, b) np-Si with porosity $\phi = 0.05$ and c) np-Si with porosity $\phi = 0.25$. All the values are normalized to the total thermal conductivity. The largest MFP contributing to heat transport for a given branch can been seen from the point where the relative cumulative thermal conductivity becomes flat.

conductivity of acoustic phonons remains essentially constant, as shown in Fig. 4-c.

Optical phonons, on the other hand, have MFPs close to L_c, and, in principle, their temperature dependence in bulk Si would affect their MFPs in np-Si. However, according to Fig. 4-b, in this temperature range, heat carried by LO phonons in bulk Si does not change significantly with temperature because the increase in heat capacity, which is shown in Fig. 4-a, is compensated by the decrease in scattering time.[2] Consequently, heat carried by LO phonons in np-Si does not change with temperature. The heat carried by TO phonons is negligible in both bulk Si and np-Si. These combined effects lead to the observed insensitivity of thermal conductivity to temperature in np-Si.

Finally, as the temperature decreases in the range 100 K $< T < 200$ K, heat carried by LO phonons in bulk Si starts to decrease, because heat capacity starts to decrease more rapidly toward lower temperatures, as shown in Fig. 4-a. As a consequence, their relative contributions to the thermal conductivity in np-Si decreases as well. According to Fig. 4-c, the decrease in the thermal conductivity is partially also due to the decrease of heat carried by the TA_2 branch because its heat capacity, as shown in Fig. 4-a, increases more rapidly with temperature than the other acoustic branches.

Although our predictions are based on np-Si, they can be applied to any Si nanostructures, as long as the feature size is comparable with the heat-carrying phonon MFPs. Notable examples belonging to this category include silicon nanowires[22], nanobridges[23] and thin films.[24]

Our results are consistent with the in-plane thermal conductivity measured over a wide temperature range for np-Si samples in which randomly arranged pores were produced by electrochemical etching 25. The sample with $\phi = 0.89$ comprises crystallites with an average dimension of 4.5 nm, similar to L_c of our structure with $\phi = 0.25$. Although the obtained temperature dependence is consistent with that from our work, the numerical value of the thermal conductivity is two orders of magnitudes lower. The reasons for such a discrepancy are explained as follows. First,according to the formula for geometric factor g above, a porosity of $\phi = 0.89$ is roughly ten times more effective in decreasing diffusive heat transport with respect to the case with $\phi = 0.25$. We note that although the formula for g has been derived for periodic pores, it can still serve as good estimator for disordered np-Si. The second reason is that in our system scattering is only from pore walls, whereas in the experiment there is also scattering by crystallite boundaries. Lastly, the experimental samples have a range of crystallize sizes, and while the average matches our characteristic size, in fact the thermal conductivity is most affected by the smallest crystallites, thus making it smaller than expected from the average. For these reasons, the experiment finds a lower overall thermal conductivity but similar temperature dependence to our np-Si results, reflecting the fact that both systems have a characteristic length much smaller than heat-carrying phonon MFPs.
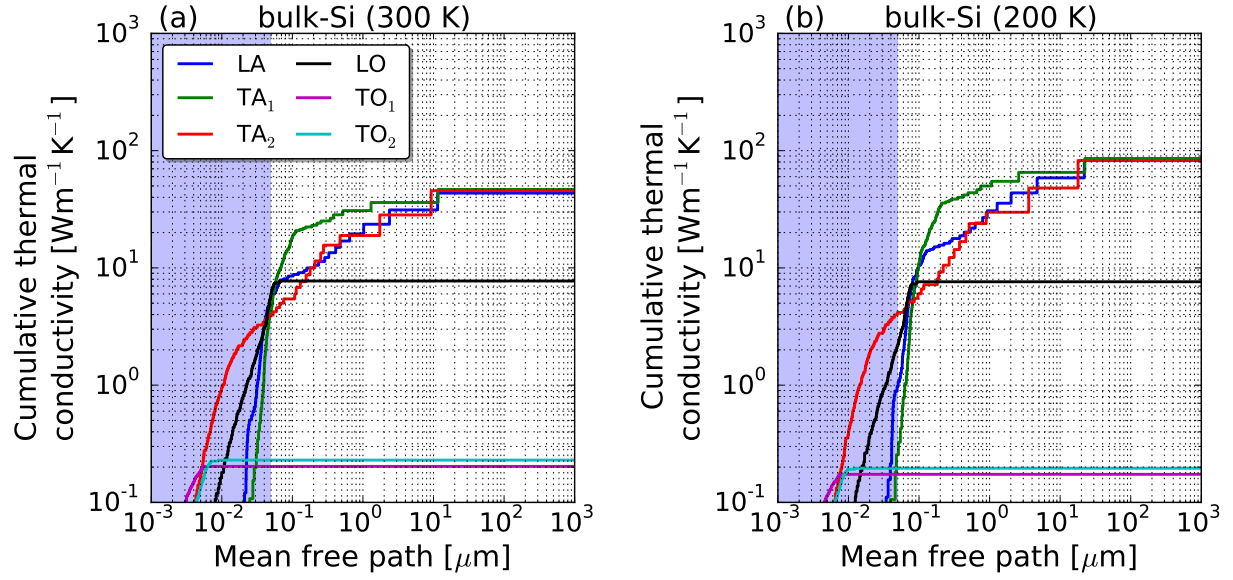
FIG. 3. MFP distributions of bulk Si at a) $T = 300$ K and b) $T = 200$ K. In both panels, the shaded area shows the region of MFPs up to ten times the characteristic size of the nanostructure in case of $\phi = 0.25$. At low temperatures, the contribution to the thermal conductivity from long-MFP acoustic phonons rises. However, the ballistic regime constrains these MFPs to be equal to L_c.
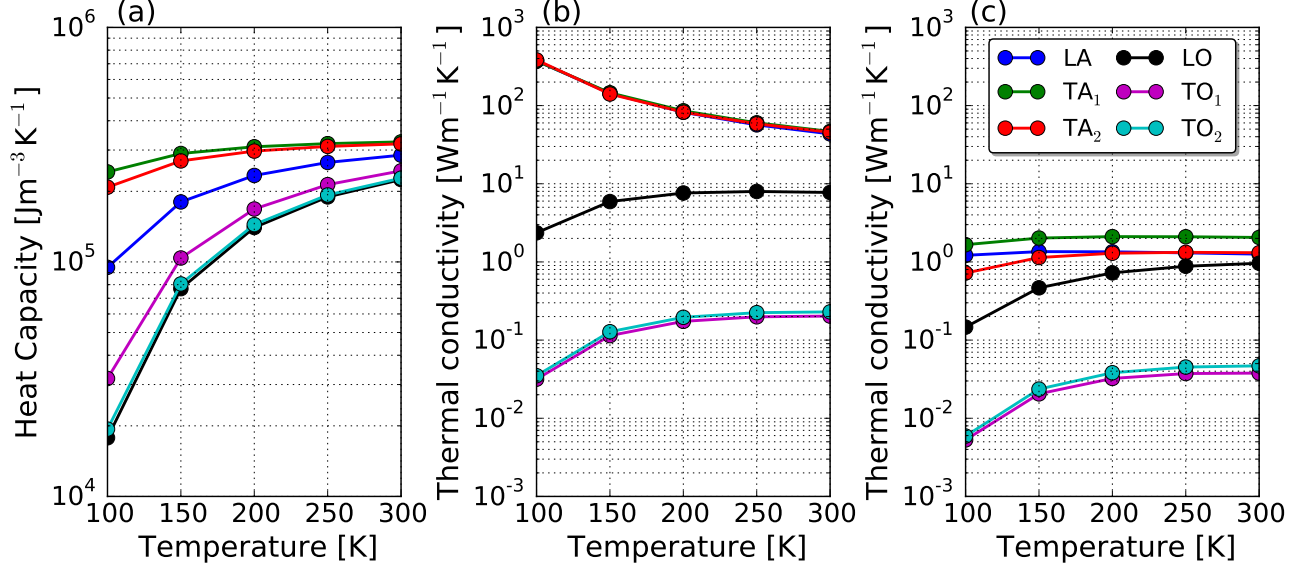

FIG. 4. a) Specific heat capacity for different phonon branches and temperatures. Contribution of each phonon branch to the total thermal conductivity for b) bulk Si and c) np-Si for $\phi = 0.25$. In the range 200 K $< T <$ 300 K, the contributions to the thermal conductivity from each phonon branch in np-Si do not change significantly with temperature. Within the ballistic regime, the temperature dependence of thermal conductivity is mainly dictated by the heat capacity.

IV.   CONCLUSIONS

Using the MFP-BTE, we calculate the temperature dependence of thermal conductivity in np-Si. We quantify the contribution of optical phonons to thermal conductivity in np-Si with periodicity 10 nm, which at room temperature amounts to 17%. We also predict constant thermal conductivity over the range 200 K $< T <$ 300 K, in qualitative agreement with experiments. Our findings help further the understanding and manipulation of heat transport at the nanoscale for low thermal-conductivity applications such as thermoelectrics. We have also showed that the effectiveness of nanostructuring in reducing thermal transport does not depend directly on the bulk thermal conductivity but rather on the bulk MFP distributions of phonon branches. Consequently, our approach suggests that the search for better nanostructured thermoelectric materials has to involve the shape of the bulk cumulative thermal conductivity in relation with the material's geometry. In other words, the material optimization has to be done at both macro and nanoscale concurrently.

V.   APPENDIX: BULK THERMAL CONDUCTIVITY

We define the cumulative thermal conductivity in the bulk material, along the x-direction, as

$$\alpha_{bulk}^p(\Lambda) = \frac{1}{(2\pi)^3} \int_{B.Z.} C_p(\mathbf{q}) v_{p,x}^2(\mathbf{q}) \tau_p^{bulk}(\mathbf{q}) \, \Theta(\Lambda - \tau_p^{\text{bulk}}(\mathbf{q}) |\mathbf{v}_{p,x}(\mathbf{q})|) d^3\mathbf{q} \tag{8}$$

where $C_p(\mathbf{q})$ is the heat capacity, $v_{p,x}(\mathbf{q})$ is the group velocity along the x-direction, $\tau_p^{\text{bulk}}(\mathbf{q})$ is the three-phonon scattering time, and Θ is the Heaviside function. We recall that the cumulative thermal conductivity is the thermal conductivity of phonons whose MFPs are below a given Λ.[14] All the quantities appearing in Eq. 8 are taken from Ref. 2 and are not reported here for the sake of simplicity. The phonon dispersion curves and scattering times are obtained by means of harmonic and anharmonic force constants, which are extracted from DFT. The system's relaxation times are computed by using a uniform reciprocal space grid of $24 \times 24 \times 24$ points, harmonic force constants up to 5$^{\text{th}}$ neighbors and cubic force constants up to first neighbors. We use the Local Density Approximation (LDA) from Perdew and Zunger[26] with a energy cutoff of 40 Ryd. The obtained bulk thermal conductivity is in good agreement with experimental data.[27]

VI.   ACKNOWLEDGEMENT

[*] romanog@mit.edu
[1] C. Vineis, A. Shakouri, A. Majumdar, and M. Kanatzidis, Adv. Mater. **22**, 3970 (2010).
[2] K. Esfarjani, G. Chen, and H. T. Stokes, Phys. Rev. B **84**, 085204 (2011).
[3] D. Song and G. Chen, Appl. Phys. Lett. **84**, 687 (2004).
[4] B. Liao, B. Qiu, J. Zhou, S. Huberman, K. Esfarjani, and G. Chen, Phys. Rev. Lett. **114**, 115901 (2015).
[5] N. K. Ravichandran and A. J. Minnich, Phys. Rev. B **89**, 205432 (2014).
[6] J.-K. Yu, S. Mitrovic, D. Tham, J. Varghese, and J. R. Heath, Nat. Nanotechnol. **5**, 718 (2010).
[7] S. Alaie, D. F. Goettler, M. Su, Z. C. Leseman, C. M. Reinke, and I. El-Kady, Nat. Commun. **6** (2015).
[8] H. Casimir, Physica **5**, 495 (1938).
[9] Z. Tian, K. Esfarjani, J. Shiomi, A. S. Henry, and G. Chen, Appl. Phys. Lett. **99**, 053122 (2011).
[10] A. M. Marconnet, M. Asheghi, and K. E. Goodson, J. Heat Transf. **135**, 061601 (2013).
[11] G. Romano and J. C. Grossman, J. Heat Transf. **137**, 071302 (2015).
[12] A. J. Minnich, J. Johnson, A. Schmidt, K. Esfarjani, M. Dresselhaus, K. A. Nelson, and G. Chen, Phys. Rev. Lett. **107**, 095901 (2011).
[13] D. Broido, M. Malorny, G. Birner, N. Mingo, and D. Stewart, Appl. Phys. Lett. **91**, 231922 (2007).
[14] D. M. Rowe, ed., *CRC Handbook of Thermoelectrics* (CRC Press, Boca Raton, FL, 1995).
[15] C. Dames and G. Chen, in *Thermoelectrics Handbook: Macro to Nano*, edited by D. M. Rowe (CRC Press, Boca Raton, FL, 2005) pp. 42–1 – 42–16.

[16] F. Yang and C. Dames, Phys. Rev. B **87** (2013).

[17] S. R. Mathur and J. Y. Murthy, J. Heat Transf. **124**, 1176 (2002).

[18] C. Ni and J. Y. Murthy, J. Heat Transf. **134**, 082401 (2012).

[19] G. Romano, A. Di Carlo, and J. C. Grossman, J. Comput. Electron. **11**, 8 (2012).

[20] G. Romano and J. C. Grossman, Appl. Phys. Lett. **105**, 033116 (2014).

[21] C.-W. Nan, R. Birringer, D. R. Clarke, and H. Gleiter, J. Appl. Phys. **81**, 6692 (1997).

[22] A. I. Boukai, Y. Bunimovich, J. Tahir-Kheli, J.-K. Yu, W. A. Goddard III, and J. R. Heath, Nature **451**, 168 (2008).

[23] A. M. Marconnet, T. Kodama, M. Asheghi, and K. E. Goodson, Nanosc. Microsc. Therm. **16**, 199 (2012).

[24] R. Venkatasubramanian, E. Siivola, T. Colpitts, and B. O'Quinn, Nature **413**, 597 (2001).

[25] G. Gesele, J. Linsmeier, V. Drach, J. Fricke, and R. Arens-Fischer, J. Phys. D: Appl. Phys. **30**, 2911 (1997).

[26] J. P. Perdew and A. Zunger, Phys. Rev. B **23**, 5048 (1981).

[27] C. Glassbrenner and G. A. Slack, Phys. Rev. **134**, A1058 (1964).